High energy primary lithium battery using oxidized sub-fluorinated graphite fluorides

M. Mar, M. Dubois, K. Guérin, N. Batisse, B. Simon, P. Bernard

High energy primary lithium battery using oxidized sub-fluorinated graphite fluorides

M. Mar[a,b], M. Dubois*[a], K. Guérin*[a], N. Batisse[a], B. Simon[b] and P. Bernard[b]

[a] Université Clermont Auvergne, SIGMA Clermont, CNRS, ICCF, 24, avenue Blaise Pascal, 63178 Aubière, France
[b] SAFT, Direction de la recherche, 111-113 Bd A. Daney, F-33074 Bordeaux, France E-

mail: Marc.Dubois@uca.fr (M. DUBOIS), katia.araujo_da_silva@uca.fr (K. GUERIN)

Abstract: Different graphite oxyfluorides were synthesized via Hummer's oxidation of sub-fluorinated graphites in order to maintain sp^2 carbon atoms available for the oxidation, C-F bonds being non-reactive. In comparison with the graphite fluoride precursors, significant improvement of the energy density in primary lithium battery is achieved when the graphite oxyfluorides are used as cathode. When the Hummer's oxidation was carried out on graphite fluoride with both $CF_{0.60}$ composition and a homogenous dispersion of non-fluorinated regions into fluorinated lattice, oxidation focused on the remaining sp^2 carbon atoms and decomposed them. Defected graphite fluorides were then synthesized. The highest ever measured energy density in primary lithium battery with fluorinated carbons as cathode, i.e. 2825 Wh.Kg^{-1}, was reached with this particular sample. Solid state NMR allowed the functional groups C-F, COC, COH, COOH and sp^2 C to be quantified in graphite oxyfluorides and fluorides and their role in electrochemical processes to be highlighted.

Keywords: Lithium-ion battery • graphite oxyfluoride • solid-gas fluorination • energy density

1. Introduction

Although promising performances as cathode in primary lithium battery, only a few works have been devoted to graphite oxyfluorides [1] [2]. For such application, most of the studies about covalent GICs concern graphite oxides (GO) [3-4] and mainly graphite fluorides (GF) [5-12] That is easily explained by high energy density 700 Wh.kg^{-1} (1000 Wh.l^{-1}), flat plateau at 2.6 V, broad operating temperature range [-40 to 90°C] and reliability on long term (20 years) recorded for Li/fluorinated carbons (CFx) systems. Nevertheless the rare works on oxyfluorides suggest high potentialities such as an energy density of 1347 Wh.Kg^{-1} for sample obtained by a two-step synthesis combining fluorination and oxidation [13] and even 2265 Wh.Kg^{-1}, thus exceeding graphite fluorides [5-12]. Fluorinated oxides were highly capacitive while oxidized fluorides have highest discharge potential despite having the same graphite precursor. Such data demonstrated that engineering the synthesis enables to modulate

the properties. Two routes may be used : i) fluorination of GO with pure molecular fluorine F_2 [14,15] or mixed medium F_2-HF-IF_5 [13] as well as liquid HF [16], [17] or solid-liquid fluorination of oxides, which enables exfoliation [18], in hot HF solution [19-21], under irradiation [22] or ii) oxidation of GF using either Brodie's [12] or Hummers' oxidation [23]. Nevertheless, Lagow concluded that GF was inert [1]. Our recent works review the two-steps syntheses of graphite oxyfluorides based on direct fluorination with F_2 and Hummers' process [24]. Both fluorination/oxidation and oxidation/fluorination sequences are efficient to prepare oxygen and fluorine rich graphite oxyfluorides, among them some are suitable for high energy cathode materials. Through both the adequate selection of precursor (GF with $CF_{0.3}$ composition in order to oxidize free carbons atoms) and control of Hummers' method temperature, homogeneous dispersions of F and O atoms were obtained at the end of oxidation/fluorination path while the reverse route results in a clear establishment of distinguished phases. Optimization of the conditions enables to reach Russian dolls structures for each crystallite from one to three parts. Inclusion of graphite core is particularly interesting for electrochemical properties in so far as oxygenated and fluorinated regions are non-conductive. Enhanced electrochemical properties of oxyfluorides were obtained for a well-defined structuration of fluoride and oxide phases together with some residual carbon phases insuring good electronic conductivity. Because of GF stability in organic electrolytes [8,9,11-13] carbon fluoride phase must be at the surface of the grain preventing from interaction in between electrolyte and electrode materials. Then, the good capacitive performances of the oxide phase can be expressed. An energy density as high as 2400 Wh.Kg^{-1} was then obtained for triphasic GF/GO/Graphite compound. With the idea to keep CFx phase as a protective, and electrochemically active, shell to avoid side reactions of GO phase with the electrolyte, oxyfluorides with different fluorine contents were synthesized. The F/C atomic ratio was fixed in the GF starting material according to the fluorination conditions (F_2 flux, duration and temperature). Moreover, the dispersion of fluorinated regions into the carbon lattice was tailored thanks to the fluorination process, either with a flux of molecular fluorine or with atomic fluorine, which is released by the thermal decomposition of a solid fluorinating agent such as terbium tetrafluoride. For different graphitized nanocarbons, nanofibers [25], nanodiscs [26] and carbon blacks [27], the fluorination mechanisms differ according to the reaction species, F_2 or $F^•$; TbF_4 allows a continuous addition of fluorine to carbon matrix and a more progressive fluorination resulting in higher homogeneity of the materials using this controlled process by comparison with the direct fluorination using fluorine gas. In other words, $F^•$ allows a homogenous dispersion of fluorinated regions into the carbon lattice to be obtained in the whole volume. With F_2 gas, fluorination occurred first on the outer tubes, discs or shells and then progressed to the core of the nanocarbons keeping the core unfluorinated for F/C lower than one. Moreover, the fluorination using TbF_4 decomposition generates the formation of an unique highly fluorinated phase, i.e. $(CF)_n$ type, whatever the fluorination temperature, the C–F bonding being covalent. $(C_2F)_n$ structural type was always present as an intermediate phase of $(CF)_n$ with molecular fluorine F_2 whatever the nanocarbon.

2. Experimental

2.1 Materials

Commercial TIMREX KS15 Graphite was purchased from Timcal. The in-plane length is about 17 µm while thickness of each platelet is about 100-200 nm. Scanning Electronic Microscopy (SEM) confirmed those data.

2.2 Direct fluorination (F_2) of graphite

Fluorination was performed by gas-solid reaction with a flux of pure F_2 gas into a nickel reactor covered with NiF_2 as a passivation layer. F_2 of 99% purity was purchased from Solvay. The fluorination of graphite was carried under static mode (closed reactor) to control the stoichiometry and to ensure homogeneity on 10 g-batch samples. Oxidation being known to mainly affect graphite phase, low fluorine contents were selected in order to achieve polyphasic compounds. So, F/C atomic ratio of 0.17, 0.30 and 0.48 were selected thanks to the reaction temperature, i.e. 355, 370 and 400°C for 3 h, respectively, compounds being denoted **DF0.17, DF0.27** and **DF0.48** (**DF** for direct fluorination). First, the reactor was purged from O_2 and moisture from air with dynamic vacuum overnight. Then, a finite quantity of molecular fluorine F_2 was introduced and the reactor was heated to the selected temperature until consumption of fluorine (i.e. pressure decrease). Finally, the reactive atmosphere was eliminated under N_2 flow after cooling of the reactor.

2.3 Controlled fluorination with atomic fluorine F•

A nickel closed reactor was used in order to preserve the defined fluorine amount (atomic and/or molecular) released by the thermal decomposition of TbF_4. A two-temperature oven was used: the part containing TbF_4 (6.2 g) was heated at 450 °C whatever the experiment whereas graphite (0.250 g) were heated at temperatures T_F of 430 and 480 °C. A reaction time of 16 h was used. Prior to the heating, a primary vacuum ($\sim 10^{-2}$ atm) was applied into the reactor. **CF0.25** and **CF0.60** were then synthesized taking into account the resulting fluorine contents of $CF_{0.25}$ and $CF_{0.60}$ (**CF** for controlled fluorination).

2.4 Hummers' oxidation.

500 mg of GF was mixed to 500 mg of $NaNO_3$ in an Erlenmeyer flask. After placing it in an ice-bath, 33 ml of concentrated H_2SO_4 were added while stirring. 3.5 g of $KMnO_4$ were carefully introduced after what the medium was heated to 35°C for 1h. Then 50 ml of distilled water were poured on with caution since the reaction is strongly exothermic. Finally, the medium was heated at 98°C for 45 min. 3 ml of H_2O_2 (30%) were added before washing-filtration process. The resulting samples are denoted **O-DF0.18, O-DF0.27, O-DF0.48, O-CF0.25** and **O-CF0.60**.

2.5 Physicochemical characterizations

X-ray diffraction (XRD) diagrams were recorded using a PHILIPS diffractometer with a Cu (K_α) radiation (λ = 1.5406 Å). NMR experiments were carried out with a Bruker Avance spectrometer, with

working frequencies for ^{13}C and ^{19}F of 73.4 and 282.2 MHz, respectively. A magic angle spinning (MAS) probe (Bruker) operating with 2.5 mm rotors was used. For MAS spectra, a simple sequence was performed with a single $\pi/2$ pulse length of 4.0 and 3.5 μs for ^{19}F and ^{13}C, respectively. ^{13}C chemical shifts were externally referenced to tetramethylsilane (TMS). ^{19}F chemical shifts were referenced with respect to $CFCl_3$.

2.6 Electrochemical tests.

The electrochemical tests were determined through galvanostatic discharges. The electrodes were composed of the sample (about 80% by weight, w/w), acetylene black (from Mersen 10%, w/ w) to ensure electronic conductivity and polyvinylidene difluoride (PVDF from Aldrich 10%, w/w) as binder. After stirring in propylene carbonate (PC), the mixture was spread uniformly onto a stainless steel current collector disk of 12 mm in diameter. Finally, after PC evaporation, the disk was heated under vacuum at 40°C then 120°C, during 1h for each temperature, to remove traces of water and solvent. A two electrodes cell was used, where lithium was both reference and counter electrodes. A polypropylene microporous film, wet with electrolyte composed of a lithium salt ($LiClO_4$ or $LiPF_6$) dissolved as 1 mol L^{-1} in PC (propylene carbonate) or a mixture of PC–EC (ethylene carbonate)-DMC (dimethyl carbonate), was sandwiched between the composite electrode and a lithium metal foil. The cells were assembled in an argon filled dried glove box. Relaxation was performed for at least 5 h until the open circuit voltage (OCV) stabilization. Galvanostatic discharges, carried out on a VMP2 from Biologic, under current density of 10 mA.g^{-1}, were acquired at room temperature between the initial OCV and 1.5 V. The discharge potential is measured at half of the discharge and is noted $E_{1/2}$.

3. Results and Discussion

Fig. 1 shows XRD diagrams for graphite fluorides precursors (**DF** series) and oxyfluorides resulting from the Hummer's oxidation; pattern of graphite oxide **GO** is shown for comparison.

All the peaks at low 2theta values are assigned to (002) reflection of lamellar materials derived from graphite. First, graphite has typical signal at 26° in 2theta corresponding to interlayer distance of 0.335 nm. Coherence length of crystallite along the c axis, Lc, collapsed from 130 nm in KS15 to 13 nm in **DF0.17**, 7 in **DF0.27** and 5 nm in **GO** (Table 1). All particles were affected by the direct fluorination or the oxidation. The values for the others samples cannot be estimated. The position of (002) reflection of $(CF)_n$ type with an interlayer distance of 0.66 nm instead of 0.6 nm for single $(CF)_n$ type underlines the presence of a mixture of $(CF)_n$ and $(C_2F)_n$; for this latter phase the expected interlayer distance is 0.8 nm. Only (001) reflection of GF phase is apparent on XRD pattern for **DF0.48** at 2theta equal to 42°, (002) reflection being ill-defined.
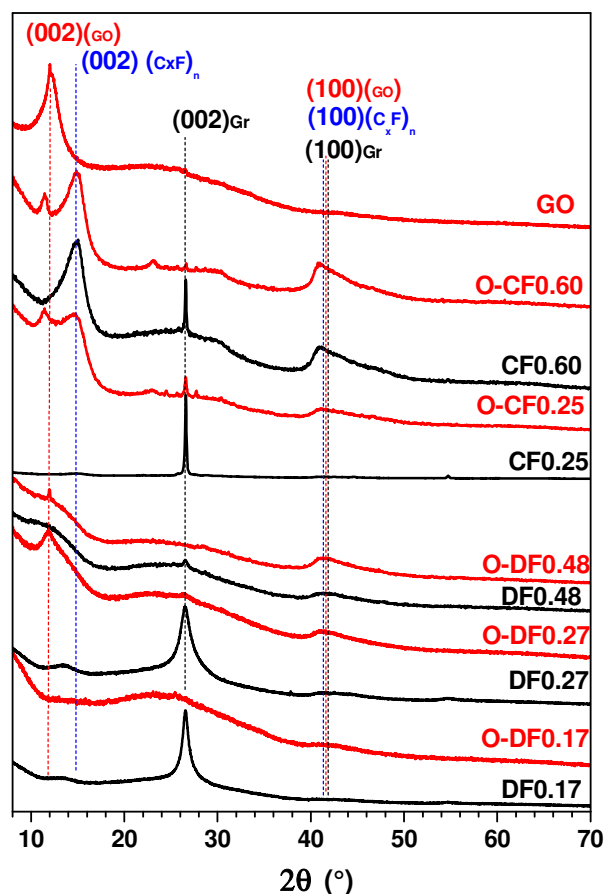
Figure 1. XRD patterns of raw and oxidized DF and CF series; GO data are added for comparison.

The differences are important after oxidation. In one hand, $(CF)_n$ phase (002) reflection at 14° seems to remain identical whatever the oxyfluoride **O-DF**. In the other hand, for the case of **DF0.27** and **DF0.17**, oxidation induces conversion of graphite phase into graphite oxide according to the total disappearance of graphite peaks (at 26 and 42°) and presence of a shoulder at 12°. The new materials are biphasic as its precursor thanks to conversion of residual graphite into graphite oxide. Graphite/$(CF)_n$ biphasic compound is converted into graphite oxide/$(CF)_n$ one, biphasic too. No evident conclusion can be done after oxidation of **DF0.48**, the XRD pattern being ill-defined. Solid state NMR will be used to further investigate this sample. XRD patterns are close for **DF0.48** and **O-DF0.48**. **GO** does not feature graphite phase peaks but only the one related to graphite oxide phase at 12°. Such a value suggests that interlayer spacing is 0.74 nm due to oxygenated functions.

Table 1. Interlayer distance and coherence length of graphite, graphite oxide GO (as reference) phases of iGO and fluorinated iGO

	Phase (reflection)	Intelayer distance (nm)	Lc (nm)
Graphite	Gr (002)	0.34	130
DF0.17	Gr (002)	0.34	13
	(CF)n (002)	0.66	--
O-DF0.17	Gr (002)		--
	GO (002)		--
	(CF)n (002)		--
DF0.27	Gr (002)	0.34	7
	(CF)n (002)	0.66	--
O-DF0.27	Gr (002)	0.34	--
	GO (002)	0.75	--
	(CF)n (002)	0.7	--
DF0.48	Gr (002)	0.34	--
O-DF0.48	Gr (002)		
	GO (002)	Ill-defined	
	(CF)n (002)	Ill-defined	
CF0.25	Gr (002)	0.34	130
	(CF)n (002)	0.60	--
O-CF0.25	Gr (002)	0.34	--
	GO (002)	0.77	--
	(CF)n (002)	0.60	--
CF0.60	Gr (002)	0.34	130
	(CF)n (002)	0.60	--
O-CF0.60	Gr (002)	0.34	--
	GO (002)	0.77	--
	(CF)n (002)	0.59	--
GO	GO (002)	0.73	5

The compound was characterized by ^{13}C MAS-NMR for quantitative data (Fig. 2a). The functional groups in the two extremes will be discussed first, i.e. GF and GO. Graphite oxide exhibits the following functional groups: epoxides COC (with chemical shift of 60 ppm), hydroxyls COH (70 ppm), sp^2 carbon in oxidized environment (sp^2 C at 135 ppm whereas pure graphitic carbon atoms result in a line at 120 ppm), and carboxyl groups COOH (165 ppm). Fits of the spectra give atomic and functional

compositions of the compounds (Table 2). GO has classical O/C ratio of 0.59 [1,4], functionalized carbons percentage %C_{fct}, i.e. all carbon atoms linked to a heteroatom (oxygen or fluorine), is equal to 63-64% (see table 2). Conduction electrons hinder the NMR measurements and lead to a significant broadening when the fluorine content is low, as for **DF0.17** and **DF0.27**. The main line at 132 ppm is assigned to sp^2 hybridized carbon atoms whereas the shoulder around 80 ppm is typical of C-F bonds [28-32]. The peak broadening is also observed on ^{19}F MAS spectrum (Fig. 2b). The main line around -200 ppm is related to covalent C-F bonds [28-32]. ^{13}C MAS-NMR are only semi-quantitative because of residual graphite phase and XPS gives the surfacic composition of $CF_{0.27}$ and $CF_{0.17}$ for **DF0.27** and **DF0.17**. The compositions were in good accordance with weight uptake during the fluorination. For the case of **DF0.48**, the fluorination level is enough to avoid perturbation due to conduction electrons, the lines being narrow and well defined at 132 ppm (non-fluorinated sp^2 C atoms in interaction with neighboring C-F), 87 ppm (covalent C-F) and 42 ppm on ^{13}C spectrum [28-32]. This latter is assigned to non-fluorinated sp^3 carbon atoms typical of $(C_2F)_n$ structural type. As a matter of fact in this structure, the stacking sequence is FCCF/FCCF, half of the carbon atoms being non-fluorinated (FCF/FCF stacking sequence for $(CF)_n$ type). The presence of the $(C_2F)n$ is also evidenced by the shoulder at -176 ppm on the main line related to covalent C-F at -190 ppm (Fig. 2b). Non-fluorinated sp^3 carbon atoms act on covalence of the C-F bonds in their neighboring. A few CF_3 (-83 ppm) and CF_2 (-115 ppm) are also present. ^{13}C MAS-NMR spectrum of **DF0.17** (Fig. 2a) being not resolute because of the low fluorine content, the resulting oxyfluorides cannot be numerically compared to the precursors. For **O-DF** series, the spectra consist in the superimposition of the lines characteristic of oxide and fluoride materials. The chemical shifts of the various groups are similar to the single phases. Epoxide (revealed by a line at 60 ppm), hydroxyl groups (70 ppm), COOH (165 ppm) and sp^2 C (around 136 ppm) coexist with covalent C-F bonds (87 ppm). ^{19}F NMR spectra are similar before and after Hummer's oxidation. Fluorine nuclei do not interact with oxygenated functions nor with sp^2 C. According to the non-reactivity of fluorinated phase, sp^2 carbon atoms seem to remain in the GO phase, probably in nanometric islands [33] rather than in graphite fluoride phase. C-F bonds, CF_2 (revealed by the presence of the line at -115 ppm) and CF_3 groups (line at -83 ppm in very low amounts) exhibit also similar chemistry in **O-DF0.17** and **O-DF0.27** in comparison with raw **DF0.17** and **DF0.27** (Fig. 2b).
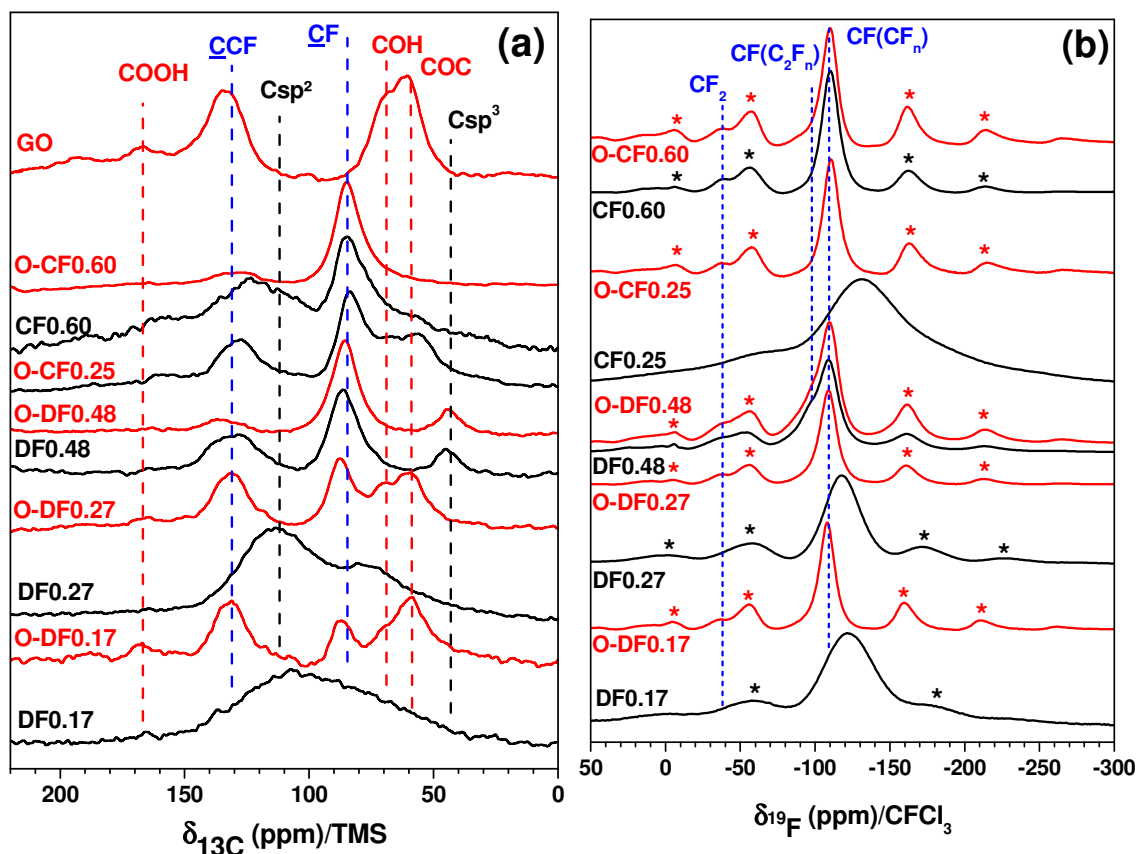
Figure 2. a) ^{13}C MAS-NMR of graphite oxide GO, DF and CF series graphite fluorides and O-DF and O-CF series oxyfluorides (10 kHz b) ^{19}F MAS-NMR of starting DF and CF precursors and resulting oxyfluorides O-DF and O-CF

The case of **DF-0.48** is different because no lines related to GO phase can be recorded after oxidation regarding ^{13}C nuclei. The only difference is the decrease of the relative content of sp^2 C atoms. The non-fluorinated sp^3 C and C-F bonds are unaffected, the ratio of their integrated lines (S_{C-F}/S_{Csp3}) being constant. Once again the fluorinated regions are not changed upon oxidation. sp^2 C atoms are consumed during the oxidation because the reaction is focused into a small part of the sample (30% of sp^2 C). Indeed, 48% are bounded to fluorine atoms, 22% are locked as sp^3 C in $(C_2F)_n$ phase. ^{19}F MAS spectra are identical for **DF-0.48** and **O-DF0.48** highlighting that both $(CF)_n$ and $(C_2F)_n$ phases are non-reactive. Increase of the fluorine content up to CF$_{0.48}$ does not allow oxyfluoride with high oxygen content to be synthesized because of the presence of $(C_2F)_n$ phase that locked 22% of the carbons in sp^3 hybridization.

Controlled fluorination with atomic fluorine allows this $(C_2F)_n$ type to be avoided in graphitized nanocarbons [25-27]; this process was carried out to prepare CF$_{0.25}$ and CF$_{0.60}$ precursors. Rather than XRD and the slight decrease of the interlayer distance at 0.6 nm, typical of $(CF)_n$ phase, ^{13}C NMR underlines the absence of $(C_2F)_n$ type because no line is observed at 42 ppm. The shoulder typical of

C-F in $(C_2F)_n$ type is not observed on ^{19}F spectrum for $CF_{0.60}$. Because the fluorinated regions are well dispersed in conductive non-fluorinated graphitic region, the resulting ^{19}F and ^{13}C spectra are ill-defined. Another consequence is the paramagnetic shift at -211 ppm of ^{19}F line for C-F bonds (-190 ppm for **CF0.60** as expected for covalent C-F bonds). An oxyfluoride is synthesized by the Hummer' oxidation of **CF0.25** since the lines of C-F (83 ppm, 34%), COC (60 ppm, 23 %), C-OH (68 ppm, 13%) and COOH (165 ppm, 2%) and sp^2 C (134 ppm, 63%) are present on ^{13}C spectrum. The same positions were recorded for **O-DF** series but the oxidation level is slightly higher for **O-CF0.25** than for **O-DF0.27** (Table 2). 72% and 63% of C atoms are functionalized by either F or O in **O-CF-0.25** and **DF0.27,** respectively.

Table 2. Atomic and functional compositions of graphite oxide, fluorides and oxyfluoride.

	O/C	F/C	%C_{fct}	%COC	%COH	%COOH	%CF
GO	0.59	0	64	37	14	13	0
DF0.17	0	0.17	17	0	0	0	17
O-DF0.17	0.43	0.12	62	33	8	9	12
DF0.27	0	0.27	27	0	0	0	0
O-DF0.27	0.33	0.25	62	14	15	4	29
DF0.48	0	0.48	48	0	0	0	48
O-DF0.48	0	0.73	73	0	0	0	73
CF0.25	0	0.25	25	0	0	0	25
O-CF0.25	0.29	0.34	72	23	13	2	34
CF0.60	0	0.60	0.60	0	0	0	60
O-CF0.60	0	0.79	79	low	low	low	≈79

Different distributions of GO, GF and graphite phases are expected in these two oxyfluorides. It is interesting to note that the relative content of COC is 23% in **O-CF0.25** significantly higher than in **O-DF0.27** (14%), the content of C-OH being close (13 and 15 %, respectively). Such differences would change the electrochemical properties as cathode in primary lithium battery. Surprisingly, no resonance line related to oxygenated group is present in **O-CF0.60** as revealed by ^{13}C NMR. Their relative contents are too low to be detected. Oxidation may result also in the decomposition of sp^2 carbon atoms. The fluorine content increased from F/C equal to 0.60 to 0.79 after oxidation because some sp^2 C are consumed by the oxidation; the relative intensity of the sp^2 C line decreases (from 40 to 21%). The fluorinated phase must be highly defected in the resulting sample, with holes where sp^2 carbons were initially present. On the contrary XRD pattern evidences the presence of a minor **GO** phase taking into account the peak around 11° with an interlayer distance of 0.77 nm (Table 1). The same conclusion can be done for **O-CF0.25**. Although **O-CF0.60** is not an oxyfluoride with high O content, it is of interest as cathode. The following section will address those properties. Scheme 1

summarizes the different samples, biphasic as **DF** and **CF** species (GF/Graphite, the first phase cited is the external part of the grain), e.g. **O-DF0.27** (GF/GO) and **O-DF0.17** (GF/GO). This biphasic structuration was expected by the control of the fluorine content in the precursors. **O-DF0.48** (defected GF/graphite), and **O-CF0.60** are particular cases and consist in defected graphite fluorides with a few oxygenated groups (not detected with ^{13}C NMR). The defects are better dispersed in **O-CF0.60** than in **O-DF0.48**. The diffusion rate of molecular fluorine within the graphite particles was controlled through the stoichiometry, the fluorination duration and the temperature [33]. The final biphasic nature is favored by the kinetics of fluorine diffusion into graphite which is one of the smallest diffusion rate in intercalation compound (D =1.45x10^{-7} cm^2.min^{-1} in HOPG). Moreover, electronegativity of fluorine implies very strong coupling with carbons [34,35].
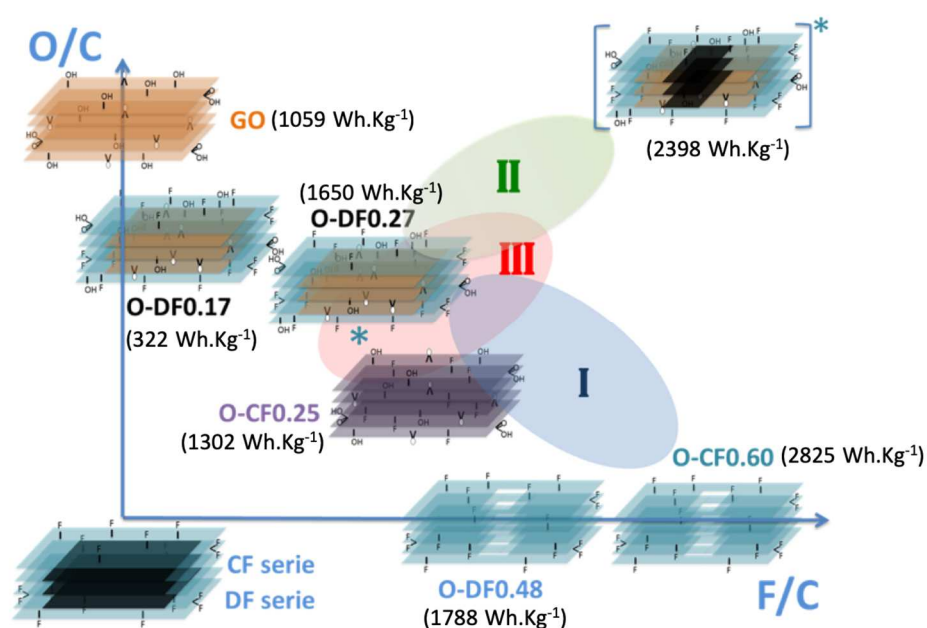
Scheme 1. Scheme of the various biphasic graphite fluorides and oxyfluorides. <mark>Zones I, II and III for further works are discussed in the text.</mark>

Mechanisms of covalent GIC graphite oxides and fluorides involve either reduction of carbon in C-F bond and then breaking of the bond liberating the fluoride anion F$^-$, which precipitates with alkaline cation Li$^+$ into LiF salts [CFx + xLi $\rightarrow$ C + xLiF] [36] or the reduction of the carbon in C-O group that leads to Li$_2$O and LiOH formation [CO$_z$(OH)$_y$ + (y+2z)Li $\rightarrow$ C + yLiOH + zLi$_2$O] [37]. The theoretical capacity C$_{theo}$ for functionalized carbon is obtained owing to the following equation: C$_{theo}$ = x*96500/(M*3.6) where x is level of functionalization of the graphite and M the active weight of the functionalized graphite.

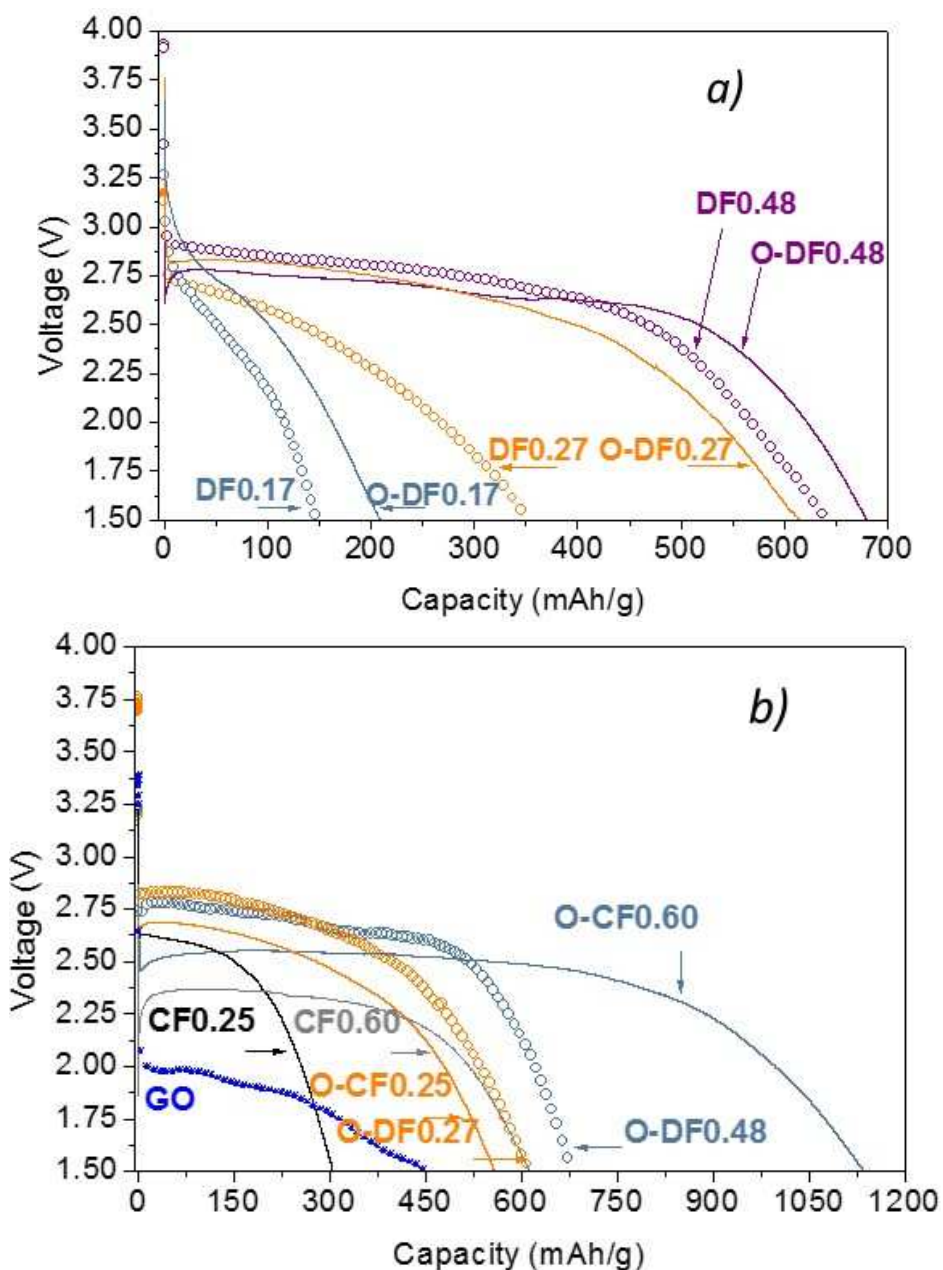**Figure 3.** Galvanostatic discharge curves at a current density of 10 mA.g^{-1} of oxides, fluoride and oxyfluorides in LiPF$_6$ 1M PC EC 3DMC.

Fig. 3 displays galvanostatic discharge curves of oxidized DF and CF series as well as the one of their precursors DF, CF and GO for comparison. Owing to the aforementioned reduction mechanism, the theoretical performances can be compared to the experimental ones. The relative contents of each electroactive groups (C-F, COC, COH) are known thanks to ^{13}C NMR (Tables 2 and 3). In accordance with the literature [36], graphite oxide GO exhibits a reduction at lower voltage (E$_{1/2}$ = 2.17 V for 64% C functionalized) than carbon fluorides (2.73 V for 48% C functionalized, i.e. for **DF0.48**). With such a potential difference, a biphasic GF/GO compounds must exhibit a galvanostatic curve with 2 well-separated plateaus especially as those latter are well defined (flat) in the pure GO and GF. On the

contrary, the discharge profiles of oxidized DF and CF do not allow the reductions of the carbon-fluorine and carbon-oxygen bonds to be distinguished. Even if the material is biphasic with carbon fluoride in surface and carbon oxide in the core, the progressive defluorination of the material sets lithium diffusion channels favorable to the reduction of the GO core of the material.

Epoxide groups are theoretically the most capacitive; however the experimental capacity is not as huge as expected. 488 mAh/g is
recorded for GO whereas 632 mAh.g^{-1} is theoretically expected Side reactions with the electrolyte may explain such a behavior that avoids the maximal capacity to be reached. The comparison between GO and O-DF0.27 validates our strategy to cover GO phase by GF, graphite fluoride being less or not sensitive to the electrolyte nature.

Table 3. Electrochemical performances of oxidized graphite fluoride compared to the ones of their respective precursors

	Theoretical capacity (mAh.g^{-1})				Exp. capacity (mAh.g^{-1})	OCV (V)	E$_{1/2}$ (V)	Energy density (Wh.Kg^{-1})
	COC	COH	CF	total				
GO	507	192	0	699	488	3.29	2.17	1059
DF0.17	0	0	0	299	184	3.26	2.22	408
O-DF0.17	416	101	151	668	210	3.45	2.48	322
DF0.27	0	0	423	423	354	3.13	2.36	835
O-DF0.27	167	179	345	691	625	3.69	2.64	1650
DF0.48	0	0	609	609	628	3.92	2.73	1714
O-DF0.48	0	0	756	756	680	3.24	2.63	1788
CF0.25	0	0	0.25	400	305	3.21	2.52	769
O-CF0.25	266	150	393	809	525	3.13	2.48	1302
CF0.60	0	0	0.60	687	612	3.10	2.31	1413
O-CF0.6	0	0	0.60	784	870	3.15	2.50	2825

The experimental capacity is higher for **O-DF0.27** (625 mAh.g^{-1}) that for **GO** (488 mAh.g^{-1}) for similar functionalized carbon percentage (62 and 64% for **O-DF0.27** and **GO**, respectively; see tables 2 and 3). Interestingly, the discharge potential is higher for the oxidized **O-DF0.27** (2.73 V) that in the precursor **DF0.27** (2.36 V). In such GO/GF biphasic compounds, the discharge potential seems to be fixed by the total functionalized carbons rather than the amount of F atoms. E$_{1/2}$ is equal to 2.63 V for **O-DF0.48** with 73% of functionalized carbons. The energy density is then enhanced to 1650 Wh.Kg^{-1}. In this series, the best material is **O-DF0.48** with a capacity of 680 mAh.g^{-1} and an energy density of

1788 Wh.Kg^{-1}. Those values exceed 628 mAh.g^{-1} and 1714 Wh.Kg^{-1} for the precursor **DF0.48**. Oxidation results in the decomposition of residual sp^2 carbon atoms and then in defected graphite fluoride with interesting properties. Such non-expected results are also obtained with **O-CF0.60** for which the fluorine content is higher. The experimental capacity of 870 mAh.g^{-1} exceeds the theoretical one (784 mAh.g^{-1}) whereas the discharge potential is still high (2.50 V). A huge energy density of 2825 Wh.Kg^{-1} is then reached. The higher fluorine content (CF$_{0.79}$) may not explain the recorded value and a synergetic effect of defects may be proposed. With the initial homogenous dispersion of sp^2 carbon regions into the fluorinated parts thanks to the controlled fluorination with atomic fluorine, the decomposition of those sp^2 islands results in a homogenous repartition of defects in graphite fluoride phase. Presence of a few residual COC is possible as evidenced by XRD; their low amounts avoid their detection by NMR. The energy density of 2825 Wh.Kg^{-1} exceeds the higher value of 2265 Wh.Kg^{-1} reported up to now (+25%). In a recent paper [24], mild oxidation of graphite fluoride with composition CF$_{0.30}$ results in energy density of 2398 Wh.Kg^{-1} with the same electrochemical conditions (electrolyte and current density). The composition of the graphite oxyfluoride was C$_{0.47}$(COC)$_{0.29}$(COH)$_{0.05}$(CF)$_{0.19}$. The enhancements have been assigned to the multiphase GF/GO/Graphite nature as an optimal stack. GF and GO are electroactive whereas residual sp^2 carbons in graphite may ensure the electron flux [38]. In other words, synergetic effects between the various functional groups and sp^2 C may occur. It is to note that the experimental capacity is significantly higher (870 mAh.g^{-1}) than theoretical value (784 mAh.g^{-1}) for the case of O-CF0.60. The first explanation is related to an overestimation of oxygenated groups using NMR data because of their low contents. On the other hand, the decomposition during the oxidation of CF$_{0.60}$ increases both porosity and specific surface area (SSA). SSA is equal to 88 m^2.g^{-1} for **O-CF0.60** whereas the value is 67 m^2.g^{-1} for **CF0.60**. Adsorption of solvated lithium ions onto this particular texture may contribute (or totally explain) to the extracapacity [39]. Moreover, the texture may play also a key role on the lithium diffusion process.

4. Conclusions

The highest ever measured energy density in primary lithium battery with fluorinated carbons as cathode, i.e. 2825 Wh.Kg^{-1}, was reached thanks to the Hummer's oxidation of graphite fluoride, with a homogenous dispersion of non-fluorinated regions into fluorinated lattice. Such a particular graphite fluoride was synthesized by a controlled fluorination with atomic fluorine released by thermal decomposition of a solid fluorinating agent (TbF$_4$). Oxidation focuses on sp^2 carbon atoms because C-F bonds are non-reactive. Decomposition occurred then in our treatment conditions resulting in defected graphite fluoride. The initial composition of CF0.60 is the more favorable and results after oxidation/decomposition in CF$_{0.79}$ composition. Even if the energy density is lower for graphite oxyfluorides, some of them exhibit promising enhancements in comparison with the graphite fluoride precursor, i.e. **O-DF0.27** exhibits an energy density of 1650 Wh.Kg^{-1}. Recently another oxyfluoride (C$_{0.47}$(COC)$_{0.29}$(COH)$_{0.05}$(CF)$_{0.19}$) was synthesized starting from graphite fluoride with close composition (CF$_{0.3}$) followed by Hummer's oxidation with milder conditions; all the steps were

performed at 0 °C [24]. This allows COC groups to be favored and sp^2 carbon islands to be maintained (see the position marked with an asterisk in Scheme 1). If similar milder conditions are applied to **CF0.60**, GO phase would be maintained allowing capacitive COC groups to be preserved and capacity improvement. The resulting oxyfluorides are located in the zone I on Scheme 1. Another strategy involves the increase of F and O contents in **CF0.25** and **DF0.27**. Durations and temperatures of fluorination and oxidation would be optimized in order to increase the percentage of functionalized carbon atoms with both F and O. Zones II and III are then covered starting with **DF0.27** and **CF0.17**, respectively (Scheme 1). Oxyfluorides and defected graphite fluorides obtained by oxidation open a new route for the development of cathode materials for high energy primary lithium battery.

References

[1] R.J. Lagow, R.B. Badachhape, J.-L. Wood, J.-L. Margrave, Some new synthetic approaches to graphite–fluorine chemistry, Dalton Trans. 12 (1974) 1268–1273

[2] V.N. Mitkin, N.F. Yudanov, V.V. Moukhin, V.V. Rozhkov, New Family of Graphite Fluoroxides-Sources for the Generation of Highly Porous, Thermally Expanded Graphites for Li Cells (Review), J. New Mat. Elect. Syst. 6(2) (2003) 103–118.

[3] H.F. Hunger, G.J. Heymach, Cathodic Discharge of Graphite Intercalation Compounds in Organic Electrolytes, J. Electrochem. Soc. 120(9) (1973) 1161–1168.

[4] R. Yazami, Stockage électrochimique de l'énergie dans les composés d'insertion du graphite, Grenoble University France, PhD thesis, 1985.

[5] O. Ruff, O. Bretschneider, Die Reaktionsprodukte der verschiedenen Kohlenstoffformen mit Fluor II (Kohlenstoff-monofluorid), Z. Anorg. Chem. 217(1) (1934) 1–18.

[6] Y. Kita, N. Watanabe, Y. Fujii, Chemical composition and crystal structure of graphite fluoride. J. Am. Chem. Soc. 101(14) (1979) 3832–3841.

[7] W. Rüdorff, G. Rüdorff, Zur Konstitution des Kohlenstoff-Monofluorids, Z. Anorg. Chem. 253(5-6) (1947) 281–296.

[8] K. Braeuer, High energy density battery, US patent 3514337, 2016.

[9] K. Braeuer, Feasability study of the lithium/CxF primary cell, R&D Technical Report ECOM-3322. 1970.

[10] M.A. Reddy, B. Breitung, M. Fichtner, Improving the Energy Density and Power Density of CFx by Mechanical Milling: A Primary Lithium Battery Electrode, ACS Appl. Mater. Inter. 5 (2013) 11207-11211.

[11] T. Nakajima, Fluorine-carbon and fluoride-carbon materials: chemistry, physics, and applications. New York: Marcel Dekker, 1995. p337.

[12] T. Nakajima, N. Watanabe, Graphite fluorides and carbon-fluorine compounds, CRC Press, 1991.

[13] I. Al-Saleh, Oxyde, fluorure et oxyfluorure de graphite : synthèse-étude structurale-propriétés électrochimiques, Clemont-Ferrand University France, PhD thesis, 1992.

[14] T. Nakajima, Y. Matsuo, Y. Morino, Discharge characteristics of fluorinated graphite-oxide, Denki Kagaku 61 (1993) 594-599.

[15] T. Nakajima, Chapter 15 "Fluorinated carbon materials for energy conversion", Nakajima T., Žemva B., Tressaud A. (Eds.), Advanced Inorganic Fluorides-Synthesis, Characterization and Applications, Elsevier, Amsterdam, 2000.

[16] L. Pu, Y. Ma, W. Zhang, H. Hu, Y. Zhou, Q. Wang, Simple method for the fluorinated functionalization of graphene oxide, RSC Adv. 3(12) (2013) 3881–3884.

[17] Z. Wang, J. Wang, Z. Li, P. Gong, X. Liu, L. Zhang, Synthesis of fluorinated graphene with tunable degree of fluorination, Carbon 50(15) (2012) 5403–5410. …

[18] M. Bruna, B. Massessi, C. Cassiago, A. Battiato, E. Vittone, G. Speranza, Synthesis and properties of monolayer graphene oxifluoride, J. Mater. Chem. 21(46) (2011) 18730–18737.

[19] T. Nakajima, Y. Matsuo, Formation process and structure of graphite oxide, Carbon 32(3) (1994) 469–475.

[20] Y. Matsuo, S. Hirata, M. Dubois, Electrochemical oxidation of graphite in aqueous hydrofluoric acid solution at high current densities, J. Fluorine Chem. 185 (2016) 36-41.

[21] O. Jankovský, P. Šimek, D. Sedmidubský, S. Matějková, Z. Janoušek, F. Šembera, Water-soluble highly fluorinated graphite oxide, RSC Adv. 4(3) (2013) 1378–1387.

[22] P. Gong, Z. Wang, Z. Li, Y. Mi, J. Sun, L. Niu, Photochemical synthesis of fluorinated graphene via a simultaneous fluorination and reduction route, RSC Adv. 3(18) (2013) 6327–6330.

[23] S. Yan, J. Zhao, Y. Yuan, S. Liu, Z. Huang, Z. Chen, Preparation and liquid-phase exfoliation of graphite fluoroxide towards graphene fluoroxide, RSC Adv. 3(44) (2013) 21869–21876.

[24] M. Mar, M. Dubois, K. Guérin, N. Batisse, B. Simon, P. Bernard, Tuning fluorine and oxygen distribution in graphite oxifluorides for enhanced performances in primary lithium battery, Carbon 141 (2019) 6-15.

[25] W. Zhang, K. Guérin, M. Dubois, Z. Fawal, D. Ivanov, L. Vidal, A. Hamwi, Carbon nanofibres fluorinated using TbF4 as fluorinating agent Part I. Structural properties, Carbon 46(7) (2008) 1010-1016; W. Zhang, K. Guérin, M. Dubois, A. Houdayer, F. Masin, A. Hamwi, Carbon nanofibres fluorinated using TbF4 as fluorinating agent Part II. Adsorption and electrochemical properties, Carbon 46(7) (2008) 1017-1024

[26] Y. Ahmad, E. Disa, M. Dubois, K. Guérin, V. Dubois, W. Zhang, P. Bonnet, F. Masin, L. Vidal, D. A. Ivanov, A. Hamwi, The synthesis of multilayer graphene materials by the fluorination of carbon nanodiscs/nanocones, Carbon 50(10) (2012) 3897-3908

[27] Y. Ahmad, E. Disa, K. Guérin, M. Dubois, E. Petit, A. Hamwi, P. Thomas, J.-L. Mansot, Structure control at the nanoscale in fluorinated graphitized carbon blacks through the fluorination route, J. Fluorine Chem. 168 (2014)163-172.

[28] A. Panich, Nuclear magnetic resonance study of fluorine–graphite intercalation compounds and graphite fluorides, Synth. Metals 100 (1999) 169-185.

[29] T. Mallouk, B. Hawkins, M. Conrad, K. Zilm, G. Maciel, N. Bartlett, Raman, Infrared and NMR Studies of the Graphite Hydrofluorides), Philos. Trans. R. Soc. London, Ser. A 314 (1985) 179-187.

[30] H. Touhara, F. Okino, Property control of carbon materials by fluorination, Carbon 38 (2000) 241-267.

[31] M. Dubois, J. Giraudet, K. Guerin, A. Hamwi, Z. Fawal, P. Pirotte, EPR and solid-state NMR studies of poly(dicarbon monofluoride) $(C_2F)_n$, J. Phys. Chem. B. 110(24) (2006) 11800–11808.

[32] J. Giraudet, M. Dubois, K. Guérin, J.P. Pinheiro, A. Hamwi, W.E.E. Stone, Solid-state F-19 and C-13 NMR of room temperature fluorinated graphite and samples thermally treated under fluorine: Low-field and high-resolution studies, J. Solid State Chem. 178 (2005) 1262-1268.

[33] A.K. Kuriakose, J.L. Margrave, Kinetics of the reactions of elemental fluorine. IV. Fluorination of graphite, J. Phys. Chem. 69(8) (1965) 2772–2775

[34] I. Palchan, D. Davidov, V. Zevin, G. Polatsek, H. Selig, Diffusion and intercalation of fluorine into highly oriented pyrolytic graphite. An in situ ESR study, Phys. Rev. B 32(8) (1985) 5554-5557.

[35] I. Ohana, I. Palchan, Y. Yacoby, D. Davidov. Raman scattering of stage 2 graphite fluorine intercalation compounds, Solid State Commun. 56(6) (1985) 505–508.

[36] P. Touzain, R. Yazami, J. Maire, Lithium-graphitic oxide cells part II: High specific surface area graphitic oxide as cathode material for lithium batteries, J. Power Sources 14 (1985) 99–104.

[37] H.F. Hunger, G.J. Heymach, Cathodic Discharge of Graphite Intercalation Compounds in Organic Electrolytes, J. Electrochem. Soc. 120 (1973) 1161–1168.

[38] R. Yazami, A. Hamwi, K. Guérin, Y. Ozawa, M. Dubois, J. Giraudet, Fluorinated carbon nanofibres for high energy and high power densities primary lithium batteries, Electrochem. Commun. 9(7) (2007) 1850-1855.

[39] S. Shiraishi, O. Tanaike, "Application of Carbon Materials Derived from Fluorocarbons in an Electrochemical Capacitor", Chapter 17, in: Advanced Fluoride-Based Materials for Energy Conversion, T. Nakajima, H. Groult, Eds., Elsevier, Amsterdam, 2015.